Time-reversal inside a granular suspension to probe ultrasound diffusion

Yamil Abraham [1,2] Bart A. van Tiggelen [3] Nicolas Benech [2] Carlos Negreira [2] Xiaoping Jia [1] and Arnaud Tourin [1,*]

[1] *Institut Langevin, ESPCI Paris, Université PSL, CNRS, Paris, France*

[2] *Laboratorio de Acústica Ultrasonora, Instituto de Física, Facultad de Ciencias, Universidad de la República, Montevideo, Uruguay*

[3] *Laboratoire de Physique et Modélisation des Milieux Condensés, Université Grenoble Alpes, CNRS, Grenoble, France*

(Received 4 March 2025; accepted 3 June 2025; published 23 June 2025)

We demonstrate that ultrasound diffusion—typically associated with the transport of average wave energy and the breaking of time-reversal symmetry—can nonetheless be revealed through a time-reversal experiment. This is achieved using an unprecedented configuration: A single piezoelectric transducer, acting as a time-reversal mirror (TRM), is buried deep inside a strongly scattering medium (a dense granular suspension), while an array of transducers is positioned at a distance, outside the scattering region. A short pulse is emitted by a single array element and the TRM records the resulting ultrasonic field, composed of a coherent ballistic wave followed by a diffuse coda wave. When the entire coda is time-reversed and re-emitted from the TRM, the wave refocuses at the original source with a focal spot size that decreases with the inverse of the TRM depth, consistent with diffusive transport. By time-reversing short coda segments at increasing times t, we observe a focal spot size scaling as $1/\sqrt{Dt}$, where D is the ultrasound diffusion coefficient. Fitting this evolution with a microscopic diffusion model allows us to extract D. Remarkably, this measurement does not require ensemble averaging, because of the inherent stability of time-reversal against statistical fluctuations.

DOI: 10.1103/47wj-s8lj

I. INTRODUCTION

Multiple scattering is a regime in which a wave propagating through a random collection of obstacles is scattered more than once. When the scattering medium becomes much larger than the scattering mean free path, the transport of energy is well described by the classical diffusion equation [1], as successfully tested for ultrasonic waves propagating in a concentrated suspension of glass beads immersed in water [2,3].

Interestingly, while the diffusion equation describes intrinsically irreversible processes at the macroscopic level, the wave equation keeps its time-reversal invariance at the microscopic scale (before averaging over disorder). In the 1990s, the reversibility of a multiply scattered ultrasonic wave (whose average energy density is described by the diffusion equation) was successfully tested using a time-reversal mirror (TRM), a device that captures a broadband wavefield and re-emits it in reverse chronological order, causing the wave to converge back to its source [4]. This study demonstrated not only that a wave can revive its past in a strongly scattering medium, but also that it can be better focused than in a homogeneous medium. As demonstrated in [5], the scattering medium can be regarded as a random lens that allows a broad angular spectrum of the source to be collected by a small-aperture TRM, even if the latter is limited to a single transducer [6]. Moreover, the more disordered the lens, the more efficient the spectrum recovery [7]. This has led to a new paradigm in wave manipulation in complex media: Contrary to long-held beliefs, disorder is not merely an obstacle to focusing and imaging but can be leveraged to control waves, as also demonstrated in optics [8–10].

Here, we advance the concept by demonstrating that a time-reversal experiment can even be used to measure the ultrasound diffusion coefficient. To achieve this, we adopt the configuration proposed by van Tiggelen [11], where the TRM is buried deep within the scattering sample. We show that this unprecedented experimental setup creates a situation where the effective aperture of the random lens is governed solely by diffusion transport, and where the size of the focal spot varies as the inverse of the size of the diffusive halo that would be created at the sample exit for a source located at the TRM position.

II. EXPERIMENT

The scattering sample consists of a random close-packed suspension of slightly polydisperse glass beads with diameters ranging from 1.4 mm to 1.6 mm [see Fig. 1(a)]. This polydispersity prevents crystallization effects, ensuring strong positional disorder. The sample is immersed in a water tank (400 mm × 150 mm × 200 mm) with beads placed at the bottom and carefully mixed before each measurement to create a new realization of disorder, achieving each time a volume fraction close to the random close-packing limit, i.e., $\phi \simeq 0.64$. Based on correlation measurements, we confirmed that these realizations are significantly independent (see Fig. S5 within the Supplemental Material [12]). An ultrasonic array of 64 piezoelectric rectangular transducer elements (separated by 0.375 mm) with a central frequency of

*Contact author: arnaud.tourin@espci.psl.eu

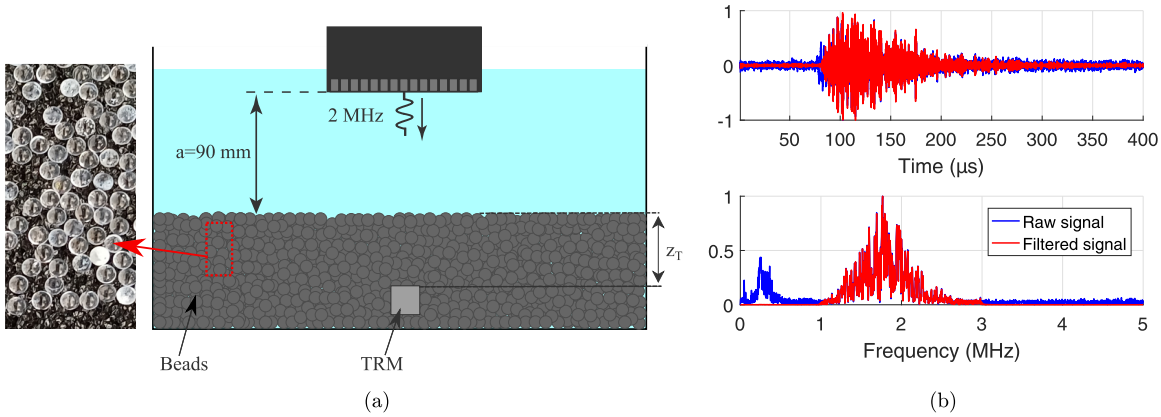

FIG. 1. (a) Schematic representation of the experimental setup. The photo shows that the beads forming the sample are not perfectly spherical and exhibit slight polydispersity (see Fig. S4 within the Supplemental Material [12]). (b) (Top) A typical waveform recorded on the TRM (in blue) is composed of a first low-frequency arrival, i.e., the ballistic coherent wave, followed by a long scattering signal, usually called the coda wave. It is frequency-filtered to suppress the ballistic wave, resulting in the signal shown in red, before time-reversal. (Bottom) Spectra of the recorded waveform before (blue) and after (red) filtering.

2 MHz is also immersed at a distance of $a = 90$ mm from the sample surface. Each element is 0.315 mm wide ($\sim$ half-wavelength in water at 2 MHz) and 15 mm high. A single rectangular transducer (0.50 mm wide and 12 mm high) with a central frequency of 1.5 MHz serves as the TRM. It is held at the bottom of the water tank at a depth z_T chosen to be much larger than the scattering mean free path, which is of the order of one bead diameter [13]. This choice ensures a diffusive regime where a source at depth z_T creates a diffusive halo with a transverse size $\sim z_T$ at the sample exit.

A time-reversal experiment is carried out in two steps. First, one element in the array is used as a source to emit a two-cycle sinusoidal wave at a central frequency of 2 MHz. The resulting transmitted waveform is then measured by the TRM. As seen in Fig. 1(b), this waveform consists of a low-frequency ballistic coherent wave (i.e., the part of the wave that would resist averaging over disorder) followed by a long scattered signal, commonly referred to as the coda wave. As evidenced by the velocity of the ballistic wave, $c \sim 1700$ ms^{-1} (close to that of water), ultrasound propagates predominantly through the interstitial fluid (water), with limited coupling to the solid skeleton of the granular packing. This behavior contrasts with that of dry granular materials, where elastic waves propagate through the heterogeneous contact network depending on the confining stress [14]. A bandpass filter, ranging from 1 to 3 MHz, is applied to eliminate the low-frequency ballistic contribution, as well as to reduce electronic noise. In the second step, a time window, called the time-reversal window (TRW), is selected from the transmitted signal and reemitted. The TRW can encompass the entire recorded signal (*stationary time-reversal experiment*), or a smaller part of it (*dynamic time-reversal experiment*).

In the *dynamic time-reversal experiments*, we set $z_T = 25$ mm and select sliding TRWs of length $T = 25$ μs, starting at time $t_w - T/2$ [shown in red in the first row of Figs. 2(a) and 2(b)]. The time step between consecutive TRWs is 5 μs, creating a 20 μs overlap. After backpropagation, the resulting time-reversed wave amplitude is recorded by all array elements and plotted as a function of space and time [second row in Figs. 2(a) and 2(b)]. The focal spot is determined from the amplitude at focusing time [third row in Figs. 2(a) and 2(b)]. Figures 2 and 3(a) illustrate how the time-reversed focal spot size decreases as the TRW is selected further into the coda wave. For the *stationary time-reversal experiment*, we need to select the longest possible TRW, at least greater than the Thouless time $z_T^2/2D$ [11]. We choose a TRW of 400 μs (limited by the noise level), approximately equal to the Thouless time for the largest TRM depth ($z_T = 25$ mm). The focal spot size is observed to vary inversely as the TRM depth [see Fig. 3(b)], indicating an isotropic diffusion regime, as discussed below.

III. THEORY

These results are well described by the microscopic diffusion theory we have developed (see the Supplemental Material [12]), the main points of which are outlined here. We assume the multiple scattering medium to be semi-infinite in the half space $z > 0$ [see Fig. 4(a)]. When a Dirac pulse is emitted from the point-like source at $\mathbf{r}_S$ (one element in the array), the signal received at the TRM at $\mathbf{r}_T$ is $G(\mathbf{r}_T, \mathbf{r}_S, t)$; i.e., the Green's function of the wave equation between points $\mathbf{r}_S$ and $\mathbf{r}_T$. A TRW $G(\mathbf{r}_T, \mathbf{r}_S, t)\mathrm{rect}(\frac{t-t_w}{T})$ is then selected, where rect is the rectangle function, time-reversed and sent back from $\mathbf{r}_T$ to the array [Fig. 4(b)]. The signal received at a position $\mathbf{r}_D$ at the array is then given by

$$F_{t_w}(|\mathbf{r}_D - \mathbf{r}_S|, t) = \left[\mathrm{rect}\left(\frac{-t - t_w}{T}\right) G(\mathbf{r}_T, \mathbf{r}_S, -t)\right] \otimes G(\mathbf{r}_D, \mathbf{r}_T, t).$$

Given the reciprocity property $G(\mathbf{r}_T, \mathbf{r}_S, t) = G(\mathbf{r}_S, \mathbf{r}_T, t)$, the focal spot size can be assessed by analyzing the variation of

$$F_{t_w}(X) = F_{t_w}(|\mathbf{r}_D - \mathbf{r}_S|, 0) = \int_{t_w - T/2}^{t_w + T/2} d\tau G(\mathbf{r}_S, \mathbf{r}_T, \tau) G(\mathbf{r}_D, \mathbf{r}_T, \tau) \quad (1)$$

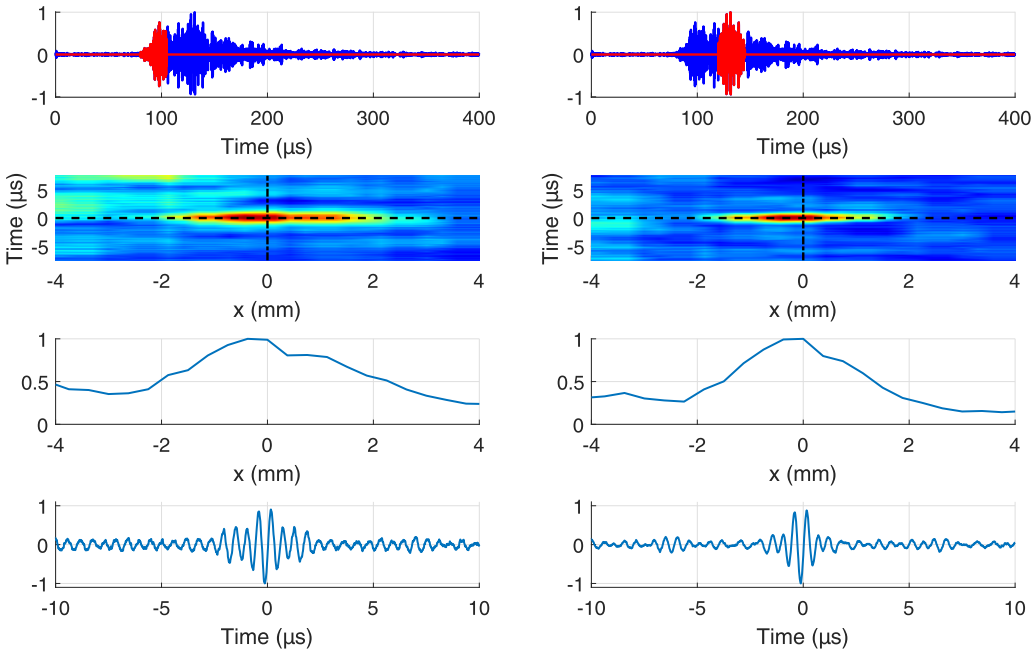

(a) $t_w = 93\,\mu s$ (b) $t_w = 148\,\mu s$

FIG. 2. Dynamic time-reversal for TRWs taken at two different times. (First row) A TRW (in red) is selected in the recorded signal and time-reversed. (Second row) The resulting time-reversed signal measured at the array is focused in both time and space. (Third row) Cross sections at the moment of focusing, defined as $t = 0$: the focal spot size is observed to decrease as a function of the TRW position. (Fourth row) The signal received back at the source is compressed in time to almost its initial duration, equal to the inverse of the bandwidth.

at the focusing time $t = 0$, as a function of the distance $X = \|\mathbf{r}_D - \mathbf{r}_S\|$ around the initial source position. This expression is a statistical estimator of the spatial correlation function $\langle G(\mathbf{r}_S, \mathbf{r}_T, t_w) G(\mathbf{r}_D, \mathbf{r}_T, t_w)\rangle$ that would be measured between points $\mathbf{r}_S$ and $\mathbf{r}_D$ for a point source located at $\mathbf{r}_T$ [6,11].

In the stationary case [which involves integrating Eq. (1) over an infinite time], the spatial correlation function can be predicted as $C(X) = \exp(-z_T kX/a)$ with k the wavenumber in the background medium (here water). This prediction is based on Akkermans and Maynard's formula for coherent backscattering (CBS) [15] generalized in [11] for a TRM placed inside a scattering medium (see Fig. S3(a) within the Supplemental Material [12]). The characteristic size of C(X), given by a/kz_T, indicates that the transverse size of the diffusive halo at the sample exit should correspond to the depth of the source within the scattering sample [see Fig. 4(c)]. The celebrated van-Cittert Zernike theorem [16] indeed states that a/kz_T is the correlation length of a wave field generated by a

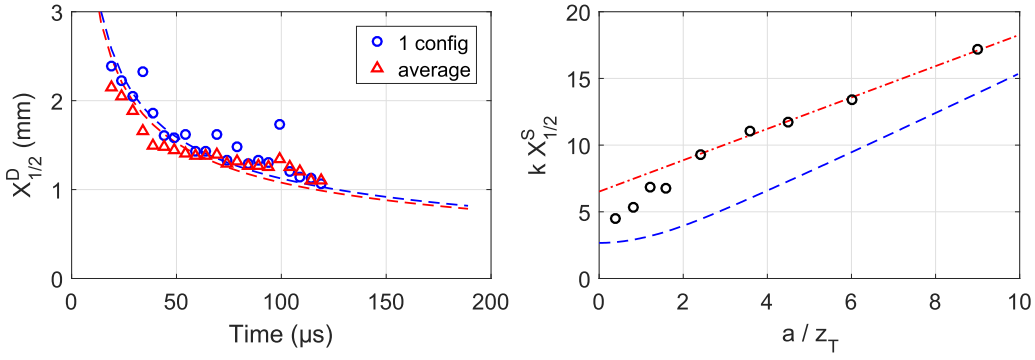

(a) (b)

FIG. 3. (a) Half-width at half-maximum of the focal spot as a function of the TRW position. Circles correspond to one realization of disorder while triangles are determined after averaging the time-reversed wave field amplitudes over eight realizations. The time axis has been shifted to align the origin with the activation time of the diffusive sources, accounting for the travel time in water. The experimental results are fitted using Eq. (3) (dashed lines). (b) Half-width at half-maximum $X^S_{1/2}$ of the focal spot as a function of TRM depth in a stationary time reversal experiment. The red-dashed line is a linear fit to the data for $a/z_T > 2$ and has slope 1.2. The theoretical prediction (blue line with a slope 1.5) takes into account the directivity of the source as well as the finite TRW size (see Fig. S3 within the Supplemental Material [12] for the influence of these parameters on the focal spot size predicted by diffusion theory).

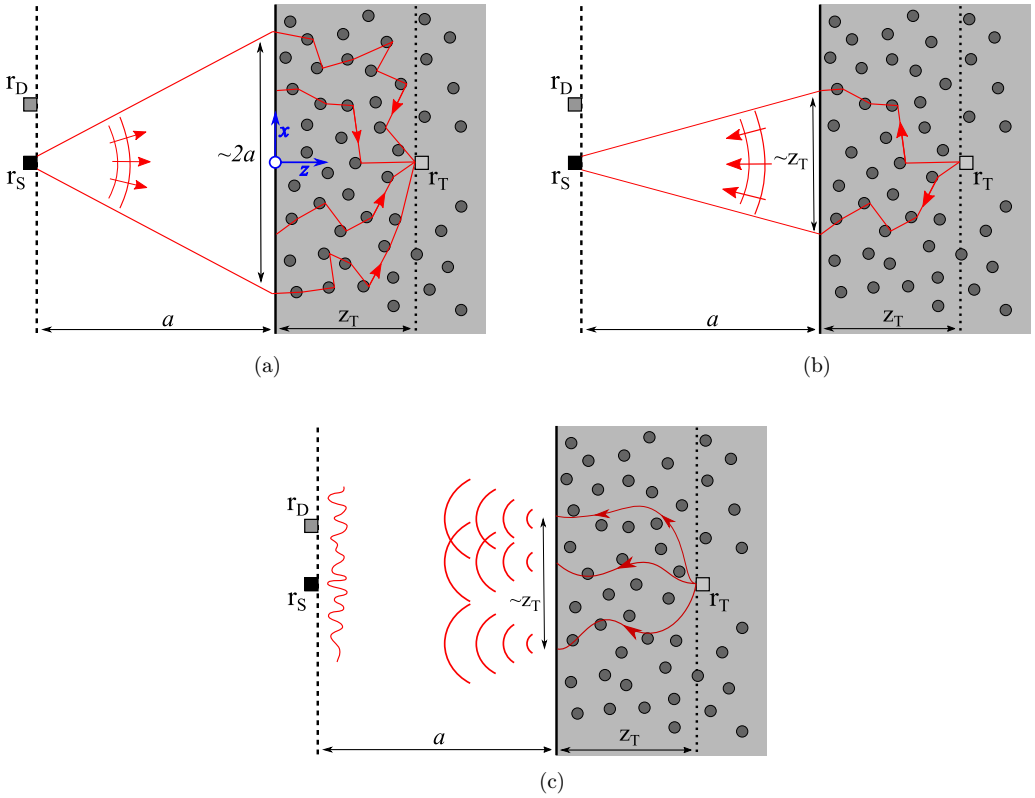

FIG. 4. Schematic diagram of the experimental set-up and coordinate system used for microscopic scattering theory. For clarity, we use dark-gray disks to represent scattering events. (a) A half-wavelength-sized source (one of the elements of the transducer array) emits a wavefront that reaches the scattering sample as a cylindrical beam with a transverse size $2a$ along x. Because of scattering, the angular spectrum of the source is redirected towards the TRM, albeit limited to a single transducer. In this sense, the sample acts as a random lens. (b) When the waveform measured at $\mathbf{r}_T$ is time-reversed and sent back, the focal spot size of the refocused signal at $\mathbf{r}_S$ is determined by the transverse size of the wavefront emerging from the sample, which in the best case is given by $2a$. (c) The focal spot size can also be viewed as an estimator of the spatial correlation function of the scattered field measured at distance a from the sample exit for a source located at z_T. In the isotropic diffusion regime, the halo at the sample exit has a size z_T and consists of random, uncorrelated sources. Consequently, the van Cittert-Zernike theorem applies, predicting a correlation length of a/kz_T provided that $a \gg z_T$.

fully spatially incoherent random source of size z_T at a distance a. In other words, in a *stationary time reversal*, the focal spot size should vary inversely with the depth of the TRM. This is what we observe as soon as $a/z_T \gg 1$ [see Fig. 3(b)], although the slope differs from the predicted ln(2) as derived from $C(X) = \exp(-z_T kX/a)$. Actually, the ln(2) slope would imply an infinite TRW as suggested by the microscopic diffusion theory we developed. When accounting for the finite size of the TRW [see blue curve in Fig. 3(b) obtained for a TRW of 400 μs as in our stationary time-reversal experiment], the agreement between experiment and theory improves. However, it remains imperfect, as the theory does not account for all experimental parameters, particularly the finite aperture of the TRM. Note that for $a/z_T < 1$, this linear dependence of the focal spot size on inverse depth breaks down due the failure of the far-field assumption. Furthermore, the y intercept is nonzero since the focal spot cannot be smaller than the initial source size. And for a source size smaller than the wavelength, the focal spot cannot be smaller than half the wavelength (diffraction limit) of ultrasound near the transducer array (i.e., in water).

For the focal spot obtained in a *dynamic time-reversal experiment*, the full calculation (see the Supplemental Material [12]) gives

$$F_t(X) \propto \int_0^{\theta_{\max}} d\theta \sin\theta J_0(kX \sin\theta) e^{-a^2 \tan^2\theta/4Dt} \times \left[\frac{e^{-z_T^2/4Dt} - e^{-(z_T+2z_0)^2/4Dt}}{(Dt)^{3/2}} \right] \tag{2}$$

with $\theta_{\max}$ fixed to $\pi/4$ by the finite directivity of the source used in our experiment.

Equation (2) predicts that the focal spot size scales as $a/k\sqrt{Dt}$ (see Fig. S2 within the Supplemental Material [12]), which indicates that the diffusion process creates a halo of size $\sqrt{Dt}$ at the sample exit. This result is reminiscent of the coherent backscattering (CBS) [17–20], especially in its dynamic version [21], consistent with the known connection between time reversal and CBS [11,22]. Quantitively, the predicted half-width at half-maximum is

$$X_{1/2}^D = \frac{0.82a}{k\sqrt{Dt}}. \tag{3}$$

IV. DISCUSSION

Fitting our data for a single realization of disorder [circles in Fig. 3(a)] to Eq. (3) yields $D = 0.61 \pm 0.08$ mm^2 μs^{-1}, with 0.08 mm^{2}μs^{-1} corresponding to the fit uncertainty. Remarkably, it appears that D can be extracted without ensemble averaging, unlike conventional methods based on time-dependent average transmitted intensity or CBS, that require averaging over disorder. Here, we leverage the stability of time reversal against statistical fluctuations [23]. Time reversal is in fact known to be a self-averaging process, as the average over disorder is replaced by an average over the number of uncorrelated pieces of information measured by the TRM, called spatial and temporal *information grains* as shown in [6]. In our case, we have only one spatial information grain (the single-channel TRM) but we have $N = T/\tau = \triangle\omega/\delta\omega = 5$ temporal/frequency information grains in the TRW (with τ the initial pulse duration, inverse of the bandwidth $\triangle\omega$, and $\delta\omega$ the decorrelation frequency). Provided that D does not vary significantly over the bandwidth, the measurement here should thus be stable against statistical fluctuations. To fully assess the statistical robustness of the method, we repeated the *dynamic time-reversal experiment* for eight realizations of disorder and found an average value of $D = 0.65$ mm^2 μs^{-1}. Notably, the dispersion around the average value, ± 0.14 mm^2 μs^{-1}, is of the same order as the fitting uncertainty for each disorder realization, confirming the statistical robustness of the method. If the time-reversed waves are themselves averaged over the 8 realizations [triangles in Fig. 3(a)], the fit of the resulting average focal spot to Eq. (3) yields a value of $D = 0.67 \pm 0.07$ mm^2 μs^{-1}, consistent with the previous measurements.

Using the same experimental setup, we also determined D using the two already mentioned conventional techniques (see details within the Supplemental Material [12]). The measurement of the dynamic CBS (for which the full 3D theory can be found in [24]) yields a value of $D = 0.70 \pm 0.03$ mm^2 μs^{-1}, while the observed time dependence of the average transmitted intensity gives $D = 0.74 \pm 0.02$ mm^2 μs^{-1}. A slight discrepancy is thus observed between the diffusion coefficients obtained from these three approaches. Each method has inherent limitations, and a detailed comparative analysis would be required to fully identify the origin of these differences, an undertaking that lies beyond the scope of this paper. Nonetheless, one possible explanation may stem from the frequency dependence of the diffusion coefficient. Indeed, all three measurements are based on pulsed experiments and thus yield values that are effectively averaged over the bandwidth of the respective signals. In the time-reversal and average transmitted intensity measurements, the detected wave fields exhibit a central frequency that is slightly downshifted (to approximately 1.75 MHz) relative to the initial pulse (centered at 2 MHz), as can be seen in Fig. 1(b). This shift can be attributed to the frequency response of the TRM, which is centered at 1.5 MHz. In contrast, the CBS measurement involves the same array for both emission and reception, resulting in a bandwidth centered around 2 MHz. Consequently, the value of D extracted from CBS is effectively averaged over a different spectral range, which may partly account for the observed variations.

V. CONCLUDING REMARKS

In this paper, we have demonstrated that a diffusion process, known to account for the transport of average wave energy and the breaking of time-reversal, can be revealed from a time-reversal method. This demonstration is based on ultrasound time-reversal experiments performed with a time-reversal mirror buried deep inside a strongly scattering medium. In this unprecedented experimental configuration, the scattering medium creates an effective aperture that is governed solely by diffusion transport. As an experimental model, we have considered a random suspension of slightly polydisperse glass beads. However, the underlying physics is generic. Since diffusion is widely recognized as a universal process, and as such hardly dependent on microscopic details, we expect our results to be broadly applicable, to any type of disordered medium (regardless of the nature of disorder) and to any type of waves as long as they propagate in the diffusive regime. In a *stationary time-reversal experiment*, we have shown that the focal spot size scales inversely with the time-reversal mirror depth, which can be interpreted as a consequence of the van Cittert-Zernike theorem. In a *dynamic time-reversal experiment*, we have demonstrated that the focal spot size shrinks as $1/\sqrt{Dt}$, where t denotes the time around which the time-reversal window is centered, i.e., the inverse transverse size of the diffusive halo at the sample exit. This offers a novel and robust way for estimating the diffusion coefficient, which, unlike conventional techniques, does not require ensemble averaging thanks to the inherent stability of TR against statistical fluctuations.

While the main purpose of this work is not to propose a new measurement technique, our findings highlight potential applications. First, it suggests that when a source is embedded in a cluttered environment—either deliberately, as in our experiment, or naturally, as with a seismic source—the spatial correlations of the scattered field it generates can be measured outside the scattering region, and used to infer the diffusion coefficient or the source depth. This approach could thus have relevance across several domains, including ultrasonic imaging of nonlinear scatterers for nondestructive evaluation [25], imaging of inaccessible interiors from their boundary, a key problem in seismology [26], as well as the localization of fluorescent emitters in optical microscopy [27,28] or quantum dots in photonic crystals [29]. Our findings also strongly resonate with recent advances in wavefront shaping [30], particularly in the context of focusing optical waves inside a diffusive medium, a field that has seen a rapid growth in the past decade [31–36]. In most of these works, the incident wavefront is shaped to match the time-reversed field of a hypothetical source located at the desired focus point.

ACKNOWLEDGMENTS

This work was supported by the French Government under the program "Investissements d'Avenir", by the Agencia Nacional de Investigación e Innovación (ANII), Uruguay, and by the Institut Franco-Uruguayen de Physique (LIA IFUP). We acknowledge Maxime Harazi who conducted the first experiments during his Ph.D. thesis.

DATA AVAILABILITY

The data that support the findings of this article are not publicly available. The data are available from the authors upon reasonable request.

[1] P. Sheng, *Introduction to Wave Scattering, Localization and Mesoscopic Phenomena* (Springer, Berlin, Heidelberg, 2006), Vol. 88.

[2] J. H. Page, H. P. Schriemer, A. E. Bailey, and D. A. Weitz, Experimental test of the diffusion approximation for multiply scattered sound, Phys. Rev. E **52**, 3106 (1995).

[3] R. L. Weaver and W. Sachse, Diffusion of ultrasound in a glass bead slurry, J. Acoust. Soc. of Am. **97**, 2094 (1995).

[4] A. Derode, P. Roux, and M. Fink, Robust acoustic time reversal with high-order multiple scattering, Phys. Rev. Lett. **75**, 4206 (1995).

[5] A. Tourin, A. Derode, and M. Fink, Dynamic time reversal of randomly backscattered acoustic waves, Europhys. Lett. **47**, 175 (1999).

[6] A. Derode, A. Tourin, and M. Fink, Random multiple scattering of ultrasound. II. Is time reversal a self-averaging process? Phys. Rev. E **64**, 036606 (2001).

[7] A. Tourin, F. Van Der Biest, and M. Fink, Time reversal of ultrasound through a phononic crystal, Phys. Rev. Lett. **96**, 104301 (2006).

[8] I. M. Vellekoop and A. P. Mosk, Focusing coherent light through opaque strongly scattering media, Opt. Lett. **32**, 2309 (2007).

[9] S. M. Popoff, G. Lerosey, R. Carminati, M. Fink, A. C. Boccara, and S. Gigan, Measuring the transmission matrix in optics: An approach to the study and control of light propagation in disordered media, Phys. Rev. Lett. **104**, 100601 (2010).

[10] A. P. Mosk, A. Lagendijk, G. Lerosey, and M. Fink, Controlling waves in space and time for imaging and focusing in complex media, Nat. Photon. **6**, 283 (2012).

[11] B. A. van Tiggelen, Green function retrieval and time reversal in a disordered world, Phys. Rev. Lett. **91**, 243904 (2003).

[12] See Supplemental Material at http://link.aps.org/supplemental/10.1103/47wj-s8lj for a detailed description of the microscopic theory, as well as additional information about the experimental setup.

[13] H. P. Schriemer, M. L. Cowan, J. H. Page, P. Sheng, Z. Liu, and D. A. Weitz, Energy velocity of diffusing waves in strongly scattering media, Phys. Rev. Lett. **79**, 3166 (1997).

[14] X. Jia, C. Caroli, and B. Velicky, Ultrasound propagation in externally stressed granular media, Phys. Rev. Lett. **82**, 1863 (1999).

[15] E. Akkermans, P. E. Wolf, and R. Maynard, Coherent backscattering of light by disordered media: Analysis of the peak line shape, Phys. Rev. Lett. **56**, 1471 (1986).

[16] J. W. Goodman, *Statistical Optics* (John Wiley & Sons, Hoboken, NJ, 2015).

[17] L. Tsang and A. Ishimaru, Backscattering enhancement of random discrete scatterers, J. Opt. Soc. Am. A **1**, 836 (1984).

[18] P.-E. Wolf and G. Maret, Weak localization and coherent backscattering of photons in disordered media, Phys. Rev. Lett. **55**, 2696 (1985).

[19] M. P. V. Albada and A. Lagendijk, Observation of weak localization of light in a random medium, Phys. Rev. Lett. **55**, 2692 (1985).

[20] G. Bayer and T. Niederdränk, Weak localization of acoustic waves in strongly scattering media, Phys. Rev. Lett. **70**, 3884 (1993).

[21] A. Tourin, A. Derode, P. Roux, B. A. van Tiggelen, and M. Fink, Time-dependent coherent backscattering of acoustic waves, Phys. Rev. Lett. **79**, 3637 (1997).

[22] J. de Rosny, A. Tourin, A. Derode, B. van Tiggelen, and M. Fink, Relation between time reversal focusing and coherent backscattering in multiple scattering media: A diagrammatic approach, Phys. Rev. E **70**, 046601 (2004).

[23] G. Papanicolaou, K. Solna, and L. Ryzhik, Statistical stability in time reversal, SIAM J. Appl. Math. **64**, 1133 (2004).

[24] L. Cobus, B. Van Tiggelen, A. Derode, and J. Page, Dynamic coherent backscattering of ultrasound in three-dimensional strongly-scattering media, Eur. Phys. J.: Spec. Top. **226**, 1549 (2017).

[25] T. J. Ulrich, P. A. Johnson, and R. A. Guyer, Interaction dynamics of elastic waves with a complex nonlinear scatterer through the use of a time reversal mirror, Phys. Rev. Lett. **98**, 104301 (2007).

[26] L. Diekmann and I. Vasconcelos, Focusing and Green's function retrieval in three-dimensional inverse scattering revisited: A single-sided Marchenko integral for the full wave field, Phys. Rev. Res. **3**, 013206 (2021).

[27] N. Irishina, M. Moscoso, and R. Carminati, Recovering fluorophore location and orientation from lifetimes, Opt. Express **21**, 421 (2013).

[28] M. P. Backlund, Y. Shechtman, and R. L. Walsworth, Fundamental precision bounds for three-dimensional optical localization microscopy with Poisson statistics, Phys. Rev. Lett. **121**, 023904 (2018).

[29] A. S. Schulz, C. A. M. Harteveld, G. J. Vancso, J. Huskens, P. Cloetens, and W. L. Vos, Targeted positioning of quantum dots inside 3D silicon photonic crystals revealed by synchrotron x-ray fluorescence tomography, ACS Nano **16**, 3674 (2022).

[30] H. Cao, A. P. Mosk, and S. Rotter, Shaping the propagation of light in complex media, Nat. Phys. **18**, 994 (2022).

[31] D. Aizik, I. Gkioulekas, and A. Levin, Fluorescent wavefront shaping using incoherent iterative phase conjugation, Optica **9**, 746 (2022).

[32] N. Bender, A. Yamilov, A. Goetschy, H. Yillmaz, C. W. Hsu, and H. Cao, Depth-targeted energy delivery deep inside scattering media, Nat. Phys. **18**, 309 (2022).

[33] R. McIntosh, A. Goetschy, N. Bender, A. Yamilov, C. W. Hsu, H. Yilmaz, and H. Cao, Delivering broadband

light deep inside diffusive media, Nat. Photon. **18**, 744 (2024).

[34] J. Liang, Z. Zhu, D. Wu, Y. Shen, J. Luo, Z. Wang, Z. Zhang, D. Qi, Y. Yao, L. Deng, F. Li, Z. Sun, Z.-C. Luo, and S. Zhang, Focusing scattered light with upconversion-nanoparticle-guided wavefront shaping, Phys. Rev. Appl. **23**, 034071 (2025).

[35] O. Haim, J. Boger-Lombard, and O. Katz, Image-guided computational holographic wavefront shaping, Nat. Photon. **19**, 44 (2025).

[36] B. A. van Tiggelen, A. Lagendijk, and W. L. Vos, Mesoscopic theory of wave-front shaping to focus waves deep inside disordered media, Phys. Rev. A **111**, 053507 (2025).